Available online at www.sciencedirect.com
SCIENCE DIRECT®

Journal of the European Ceramic Society 23 (2003) 2947–2954

www.elsevier.com/locate/jeurceramsoc

Texture of MBE grown Cr films on α-Al_2O_3(0001): the occurrence of Nishiyama-Wassermann (NW) and Kurdjumov-Sachs (KS) related orientation relationships

S. Tsukimoto, F. Phillipp, T. Wagner*

Max-Planck-Institut für Metallforschung, Heisenbergstraße 3, D-70569 Stuttgart, Germany

Abstract

The orientation and texture of Cr(110) films on the basal plane of α-Al_2O_3 was investigated by transmission electron microscopy. The Cr was deposited via molecular beam epitaxy at a substrate temperature of 110 °C resulting in the formation of crystallites with columnar mophology. Two orientation relationships (OR) were observed between Cr(110) and α-Al_2O_3(0001): Cr[001] // α-Al_2O_3[$\bar{1}$10] and Cr[$\bar{1}$11] // α-Al_2O_3[$\bar{1}$10]. Each of these orientation relationships exhibited two variants which were rotated ±5.26° around the substrate normal. The orientation relationships can be rationalized on the basis of geometry, rotational symmetry and lattice mismatches of the Cr/(110)/α-Al_2O_3(0001) interface. The occurrence of all OR can be related to Nishiyama-Wassermann (NW) and Kurdjumov-Sachs (KS) orientations and are discussed with respect to previous experimental results and geometrical parameters of other bcc metals which were grown on α-Al_2O_3(0001).
© 2003 Elsevier Ltd. All rights reserved.

Keywords: Lattice; Microstructure; Substrates

1. Introduction

Metal films on oxide substrates are of great importance for a variety of scientific problems and technological applications. Frequently, the defect density in the film should be low and, in addition, the film should be stable against chemical reactions with the substrate, i.e. interdiffusion or the formation of interfacial phases. The demands become more and more critical since film thicknesses are continuously reduced for specific applications. To fulfill these conditions, thin metallic buffer layers can be introduced between the actual metal film and the oxide substrate. The suitable buffer layer should enhance adhesion, reduce the defect density in the deposited metal film and may also serve as a diffusion barrier. Metallic buffer layers have a high reactivity or a fairly high oxygen affinity, examples are Nb, Cr or Ti. In comparison to noble metals, such as Cu and Pt, reactive metals wet the oxide substrates quite well, and favor the formation of films that cover the substrate at thicknesses of only a few monolayers.[1–3] For film growth on single crystal substrates, the formation of epitaxial films with very low defect densities is possible.[2] However, the occurrence of epitaxy may be limited by the deposition temperature and growth rate.

So far, growth studies of a variety of reactive metals (Nb, Mo, V) with bcc structure on the basal plane of α-Al_2O_3 have been performed.[4–16] These studies revealed that the epitaxial growth of the metals is strongly influenced by the growth temperature, the deposition rate and the surface preparation of the substrate. Depending on substrate orientation, at temperatures below 200 °C, bcc metals tend to grow with a {110} texture, whereas at high growth temperatures, epitaxial films with a {111} orientation may be formed.

The present study is part of a more detailed investigation of the nucleation and growth of Cr clusters and films on the basal plane of α-Al_2O_3 at different substrate temperatures. Cr is a transition metal with bcc structure and exhibits a variety of interesting optical, magnetic and electrical properties.[17–21] Despite the importance of these films for specific applications, only a few microstructural investigations of Cr films on α-Al_2O_3 have been conducted to date. So far, details on the orientation of Cr crystallites or films with respect to the orientation of the substrate were not reported.

* Corresponding author. Tel.: +49-711-689-3434; fax: +49-711-689-2412.
E-mail address: wagner@mf.mpg.de (T. Wagner).

0955-2219/03/$ - see front matter © 2003 Elsevier Ltd. All rights reserved.
doi:10.1016/S0955-2219(03)00306-6

In this paper, we report on the morphology and microstructure of a Cr film grown at 110 °C. In particular, the geometrical orientation relationships of individual Cr crystallites with respect to the α-Al_2O_3(0001) substrate are investigated by imaging and diffraction studies in the transmission electron microscopy (TEM). The results are discussed in terms of lattice mismatches [22] between Cr and α-Al_2O_3 along specific in-plane directions. Finally, the results are compared with similar metal/α-Al_2O_3(0001) systems.

2. Experimental

Cr films were grown in a commercial molecular beam epitaxy (MBE) system (Metal 600, DCA Instruments) with a base pressure of $\sim 1\times10^{-8}$ Pa. The system consists of a growth chamber equipped with a reflection high-energy electron diffraction system, a sputter cleaning chamber with a Kaufmann type ion source, and an analysis chamber encompassing an Auger system. Commercially cut and polished α-Al_2O_3(0001) single crystals, with dimensions $10\times10\times1$ mm^3, were used as substrate material. The substrate was cleaned in an ultrasonic bath with high purity acetone and alcohol prior to mounting on a Ta holder. The substrates were bombarded with Ar ions and subsequently annealed for 2 h at 1000 °C. This cleaning procedure removes C and Ca impurities from the surface and restores the surface crystallography. After this surface preparation procedure, the concentration of surface contaminants was below the detection limit of the Auger system (estimated to be approximately 0.01 monolayer of Ca and C). As shown by reflection high-energy electron diffraction (RHEED), the α-Al_2O_3(0001) surface was unreconstructed. Chromium (99.99 at.% Cr) was deposited onto the cleaned α-Al_2O_3(0001) surface via electron beam evaporation at a rate of 0.07 nm/s and a substrate temperature of 110 °C. This temperature was chosen to eliminate the influence of substrate heating by the deposition source. The thickness of the Cr films was selected to 70 nm for all films. During evaporation, the residual gas pressure in the deposition chamber was about 10^{-7} Pa.

During growth, the epitaxial relation between Cr and sapphire was characterized by RHEED. Detailed information on the microstructure of the films, including the Cr/sapphire interface, could be obtained by transmission electron microscopy (TEM). Prior to the TEM analysis, specimens for plan-view and cross-sectional observations were prepared by common procedures described by Strecker et al. [23] For conventional TEM investigations, a JEM-4000 FX (Jeol) operated at an accelerating voltage of 400 kV was used. High-resolution TEM (HRTEM) investigations were performed in a JEM-1250ARM (Jeol), operated at 1250 kV.

3. Results

Fig. 1(a) shows a plan-view bright field TEM micrograph of the Cr film grown on the α-Al_2O_3 substrate. The incident electron beam is parallel to the $[0001]_S$ direction (S = sapphire (α-Al_2O_3)). The Cr film is polycrystalline and consists of individual grains with a diameter of 5 to 20 nm. In the individual grains, Moiré fringes are visible, which are caused by an overlap of the Cr grains and the alumina substrate. A selected area diffraction (SAD) pattern of the Cr film on the α-Al_2O_3 is shown in Fig. 1(b). The hexagonal arrays of spots

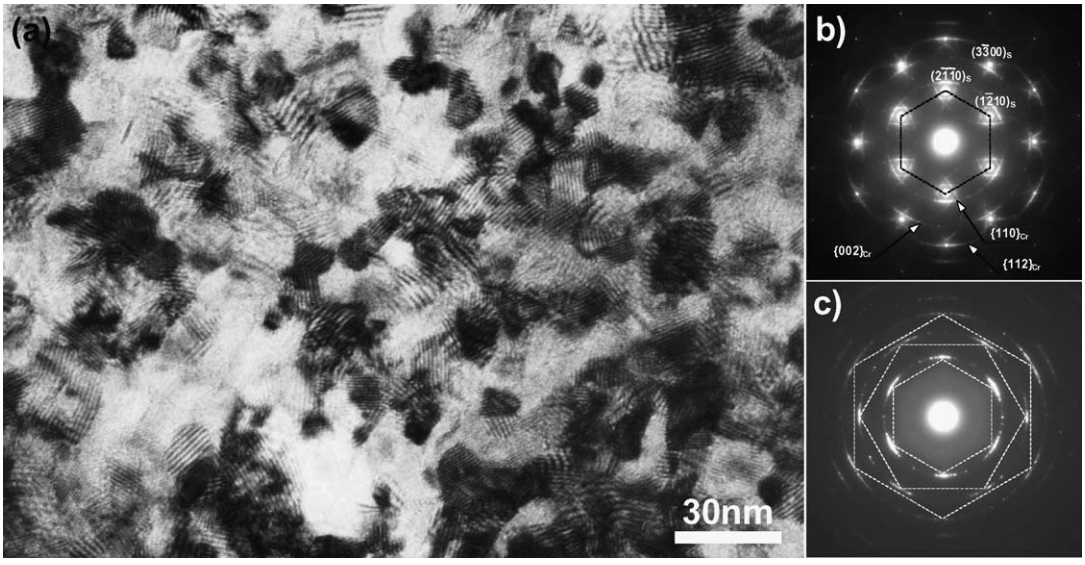

Fig. 1. Microstructure of the Cr film grown on the α-Al_2O_3(0001): (a) Plan-view bright field TEM micrograph, viewed perpendicular to the interface. (b) SAD pattern of the Cr film on the substrate. (c) SAD pattern of the Cr film without the substrate.

around the central beam, which are—for better visibility—connected with a black dotted line, are $\{\bar{2}110\}_S$ type reflections originating from the sapphire oriented parallel to the $[0001]_S$ zone axis. In addition, arc-shaped reflections around the substrate spots are visible, which correspond to {110}, {200}, and {112} type reflections, respectively, of the Cr film. Additional reflections are visible, which are caused by double diffraction between the film and the substrate. A diffraction pattern from the Cr film alone can be seen in Fig. 1(c). As indicated by the white hexagonal dotted lines, the arc-shaped patterns have a six-fold rotational symmetry similar to the patterns originating from the substrate. This reveals that the Cr film has a strong fiber texture with a preferred in-plane rotational orientation around the $[110]_{Cr}$ zone axis. A more detailed analysis of the orientation relationship (OR) between Cr and sapphire was performed via cross-sectional TEM investigations and is presented next.

Fig. 2(a) shows a cross-sectional bright field micrograph of the Cr film with the incident beam direction parallel to $[\bar{1}10]_S$. The Cr film thickness is quite uniform and approximately 70 nm, as expected. As can be seen from the contrast in the film, the Cr film consists of individual columnar shaped crystallites which are oriented perpendicular to the interface. A SAD pattern recorded from the Cr/α-Al_2O_3 interfacial region can be seen in Fig. 2(b). Fig. 2(c) shows a schematic diagram of this diffraction pattern, where full and open circles represent reflections from the Cr grains and the α-Al_2O_3 substrate, respectively. As indicated by the solid and dotted lines, Cr crystallized with two different orientation variants, OR-I and OR-II, on the (0001) α-Al_2O_3 plane:

OR-I: $(110)_{Cr}$ // $(0001)_S$
$[001]_{Cr}$ // $[\bar{1}10]_S$

OR-II: $(\bar{1}10)_{Cr}$ // $(0001)_S$
$[\bar{1}\bar{1}1]_{Cr}$ // $[\bar{1}10]_S$

These orientations are identical to those observed in the plan view TEM sample (Fig. 1). It should be pointed out that only a few grains possessed this perfect epitaxial orientations; the other grains were rotated around the $[110]_{Cr}$ axis (compare Fig. 1). A HRTEM micrograph from the interfacial region between the Cr film and the $(0001)_S$ substrate can be seen in Fig. 3. The incident electron beam is parallel to $[\bar{1}10]_S$. On an atomic level, the Cr/α-Al_2O_3 interface is quite flat and abrupt. The residual roughness and steps (see arrow in Fig. 3) at the interface originate from the α-Al_2O_3(0001) surface preparation. No intermediate interfacial phases could be detected. $(110)_{Cr}$ lattice fringes of 0.20 nm in distance, which run parallel to the interface, are clearly resolved. The epitaxial orientation variants described above can be seen in Fig. 3 and are marked with 'M' and 'N', respectively. The boundaries of the Cr grains, however, are not clearly resolved. The grains are overlapping in such a way that the grain boundaries are not oriented edge-on along the beam direction. In addition, some Cr grains are tilted away from the $[001]_{Cr}$ and $[111]_{Cr}$ zone axes, as already observed in Fig. 1.

On the basis of the aforementioned epitaxial OR, we constructed a stereographic projection, with viewing directions parallel to $[110]_{Cr}$ and $[0001]_S$,respectively (Fig. 4). The two different orientation variants OR-I and OR-II are presented in Fig. 4(a) and (b), respectively. The full circles, the open squares and the hexagons denote different directions of the Cr and sapphire,

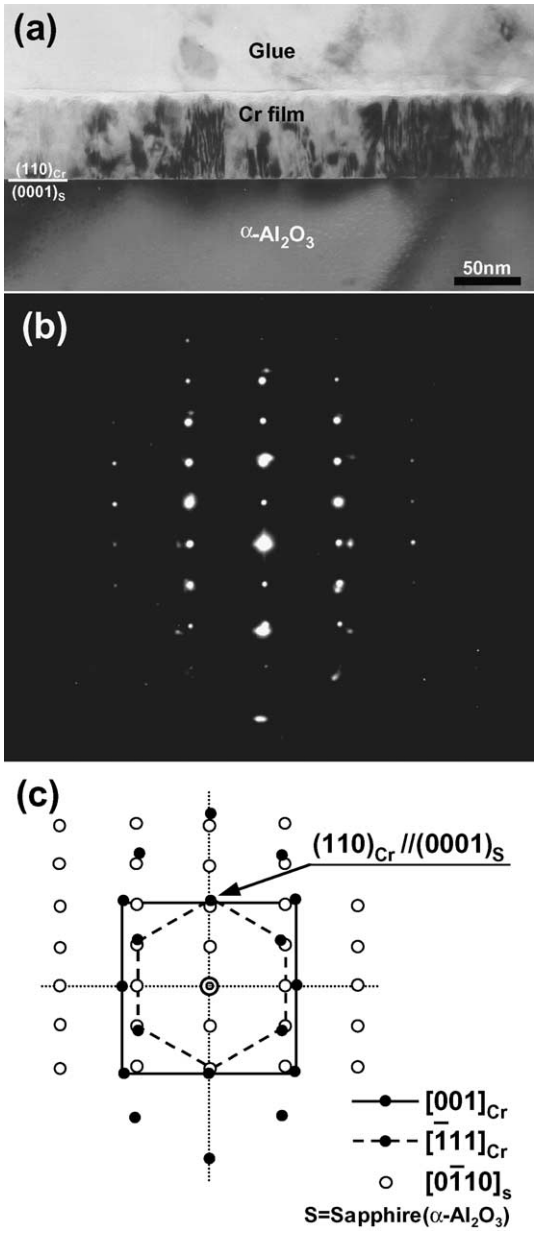

Fig. 2. (a) Cross-sectional bright field TEM micrograph of the Cr/α-Al_2O_3 interface viewing along α-$Al_2O_3[\bar{1}10]$. (b) SAD pattern of the interfacial region. (c) Schematic diagram of (b).

respectively. As depicted in Fig. 4, a rotation of $\pm 5.26^\circ$ around the common $[110]_{Cr}$ and $[0001]_S$ axis transforms OR-I into OR-II. As a consequence of OR-II, the $[\bar{1}13]_{Cr}$ and $[11\bar{2}0]_S$ directions [Fig. 4(b), symbol '*'] are only rotated by approximately 0.5° with respect to each other.

Fig. 5 shows schematically the generation of the plan view diffraction pattern, including reflections from the substrate and Cr crystallites with different orientations. The Cr(110) surface has a two-fold rotational symmetry, while the α-Al_2O_3(0001) has a three-fold symmetry. Regarding OR-I, three symmetrically equivalent orientation variants of Cr(110) are possible [Fig. 5(a)]. The rectangular dotted lines, marked by A, B and C, indicate the arrays of reflections from each of the three variants. As pointed out above, by rotating the diffraction spots of the Cr variants by $\pm 5.26^\circ$ around the central beam, the diffraction pattern of OR-II can be

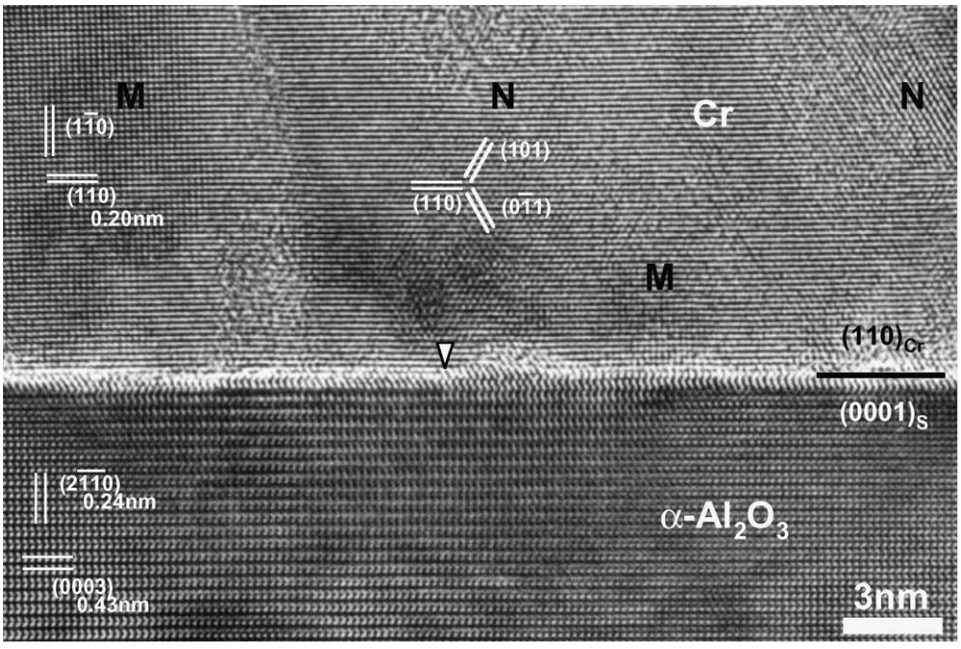

Fig. 3. HRTEM image at the Cr(110)/α-Al_2O_3(0001) interface viewing along α-$Al_2O_3[\bar{1}10]$. M and N represent grain variants with two different orientation relationships of OR-I and OR-II, respectively. The substrate surface exhibits a step structure as indicated by the arrow.

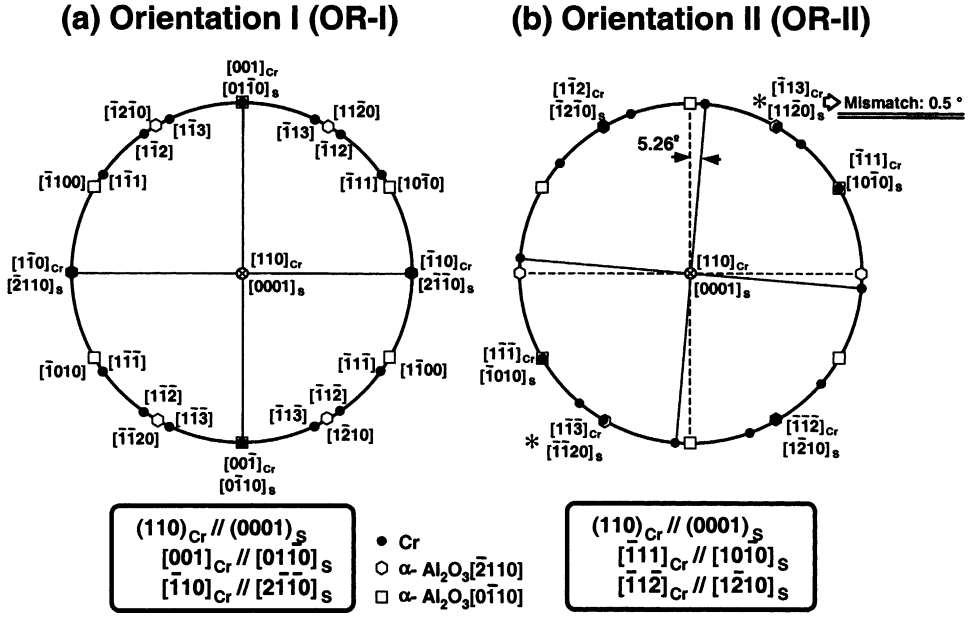

Fig. 4. Stereographic projections of in-plane geometrical orientations of (110)-oriented Cr film: (a) OR-I, and (b) OR-II.

obtained. A diffraction pattern from the substrate and OR-I and OR-II is shown in Fig. 5(b). Together, the three variants of OR I and OR II lead to nine well-defined orientation relationships between Cr and sapphire. The adjacent spots, originating from Cr, are very close together. Therefore, we could not distinguish the individual spots. Overlapping of these individual spots results in a pattern with arc-shaped spots [Figs. 1(b) and 5(c)].

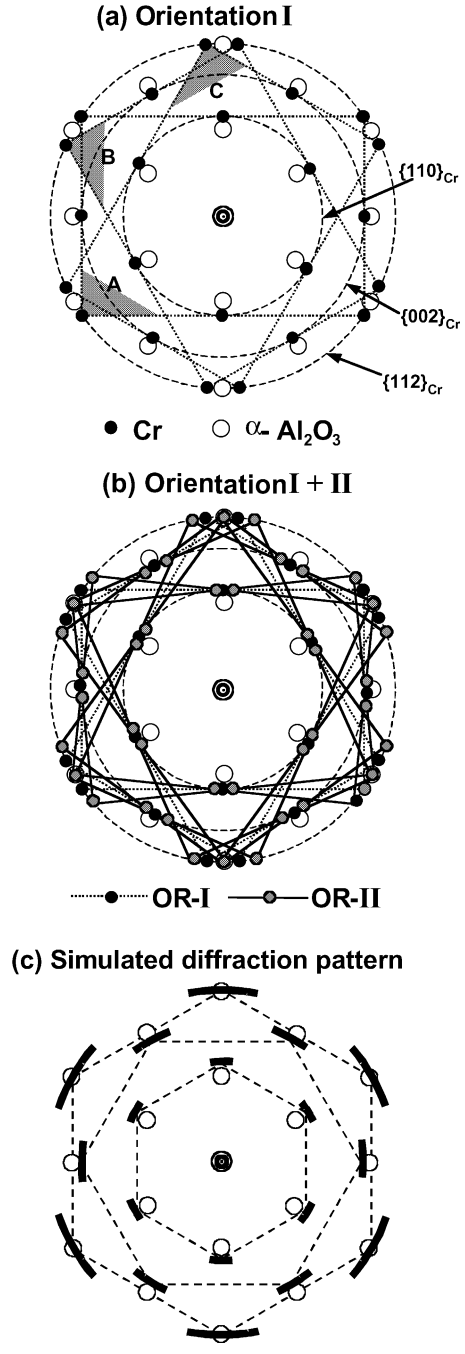

Fig. 5. Schematic of plan-view diffraction pattern: (a) OR-I with three equivalent variants A, B and C, (b) mixture of OR-I and OR-II, rotated by $\pm 5.26^{\circ}$ around the common axis of $[110]_{Cr}$ and $[0001]_S$, and (c) simulated pattern with OR-I and OR-II.

4. Interpretation and discussion

4.1. Texture formation

In the present study, a (110)-textured Cr film grew on the basal plane of sapphire. It is well-known that the microstructure of metal films grown by MBE depends strongly on growth conditions such as substrate surface structure, growth rate and substrate temperature. The surface defects and contaminants influence the nucleation, growth and therefore the final microstructure of the thin film. This may change the adsorption energy, the surface diffusion, and/or the nucleation site densities, resulting in the development of a specific thin film texture.[24–26] In the present experiment, our substrates were fairly clean (AES measurements). This implies that the development of the orientation of the Cr film on the sapphire substrate are influenced by the growth temperature and deposition rate. Detailed growth studies are available for the growth of Nb on the sapphire basal plane.[4–12] Cr and Nb posses the same crystal structures and have similar oxygen affinities.[27] However, the lattice parameters of Cr and Nb are quite different. Nevertheless, to gain a more detailed insight in the nucleation and growth processes, it is reasonable to compare Nb growth studies with our present results. From this comparison trends about the influence of lattice mismatches between metal and α-Al_2O_3 (0001) on epitaxy can be deduced. For example, low deposition temperatures (RT) lead to the development of a (110)-textured Nb film on α-Al_2O_3 (0001) (e.g. [7,14]), whereas at fairly high temperatures (several hundred °C) a well-defined epitaxial orientation relationship was observed, where (111) Nb was parallel to α-Al_2O_3 (0001) .[11] This orientation relationship may be favored by a low lattice mismatch $f(\%) = 100(d_s - d_{bcc})/d_{bcc} = 2.0\%$.[22] A low lattice mismatch results in a lower density of interfacial defects and therefore in a lower interfacial energy. A comparison between Nb and Cr films on α-Al_2O_3 (0001) suggests, that the mobility of the Nb and Cr adatoms at 110 °C was rather low, resulting in crystallite orientations, that are dominated by the low energy of the $(110)_{Metal}$ surfaces, i.e. the adatoms did not have enough kinetic energy to reach low energy positions at the interface. Nevertheless, the (110) oriented Cr clusters have an in plane orientation which may be favored by low lattice mismatchs of $f = -4.8\%$ and $f = 1.0\%$ along the $[001]_{Cr}$ and $[\bar{1}11]_{Cr}$ directions, respectively (Table 1).

OR-I for Cr is similar to the orientation relationship found by Cuomo and Angilello [4] and Mašek and Matolín [12] for (110)-aligned Nb grains on $(0001)_S$. In the case of Nb, OR-I seems to be favored by a fairly low lattice mismatch of $f = 2.0\%$ between $(\bar{1}10)_{Nb}$ and $(2\text{-}1\text{-}10)_S$ planes whereas the corresponding misfits are too large to favor ORII (Table 1).

Table 1
Lattice mismatch between bcc metal (110) and α-Al_2O_3(0001) in the two orientation relationships OR-I(NW) and OR-II (KS), where negative and positive signs of the values represent compressive and tensile stress due to mismatch, respectively

Orientation relationship (OR)		Mismatch f (%)				
		Nb	Mo	V	Cr	Fe
NW (OR-I)	$(002)_{Me}//(03\bar{3}0)_S$	−16.7	−12.7	−9.6	−4.8	−4.1
	$(\bar{1}10)_{Me}//(2\bar{1}\bar{1}0)_S$	+2.0	+6.9	+10.7	+16.6	+17.4
KS (OR-II)	$(\bar{1}11)_{Me}//(30\bar{3}0)_S$	−27.9	−24.4	−21.7	−17.5	−17.0
	$2\times(\bar{1}12)_{Me}//(\bar{1}\bar{2}10)_S$	−11.9	−7.4	−4.1	+1.0	+1.7

4.2. Orientation of individual crystallites

It is well accepted that the substrate surface termination can influence nucleation and growth processes. The α-Al_2O_3(0001) surface may be either oxygen- or aluminum-terminated .[28] Up to now, experimental and theoretical investigations of the α-Al_2O_3(0001) surface could not unequivocally determine which surface termination is present after sputter cleaning and annealing in UHV at high temperatures[28–32] and which surface termination is present after metal film deposition.[8,11,15,29,32,33] For simplicity, we assume that the α-Al_2O_3 at the Cr/α-Al_2O_3 interface is oxygen-terminated. Fig. 6 represents a schematic picture of the unreconstructed oxygen terminated substrate surface (top view). The oxygen surface sublattice is close-packed. The unit cell of α-Al_2O_3 is marked by A (dotted line), whereas the surface unit cell, relying on the oxygen termination, is denoted as B (solid line) (Fig. 6). The symmetry of cell B is equivalent to that of a fcc{111} and hcp{0001} surface. The orientation relationships between A and B are denoted in Fig. 6. Following this relationship, the $[\bar{1}10]_S$ and $[\bar{2}110]_S$ directions are parallel to fcc$<\bar{1}10>$ or hcp$<\bar{2}110>$, and fcc$<11\text{–}2>$ or hcp$<\bar{1}10>$, respectively. A variety of experimental and theoretical studies of the bcc(110)/fcc(111) and bcc(110)/hcp(0001) orientation relationships can be found in the literature (e.g. [34,35]). In metal-metal systems, two specific ORs are known as Nishiyama-Wassermann (NW) [36,37] and Kurdjumov-Sachs (KS) orientations,[38] respectively. To allow a treatment of the Cr/α-Al_2O_3 epitaxy within the geometric approach, which was developed for the analysis of bcc/fcc epitaxy (e.g. [39]), it is reasonable to transform OR-I and OR-II into OR-IT and-IIT as follows:

(OR-IT) $(110)_{Cr}$ // fcc (111) or hcp(0001)
$[001]_{Cr}$ // fcc[1–10] or hcp$[\bar{2}110]$

(OR-IIT) $(110)_{Cr}$ // fcc (111) or hcp(0001)
$[1\text{–}11]_{Cr}$ // fcc[1–10] or hcp$[\bar{2}110]$

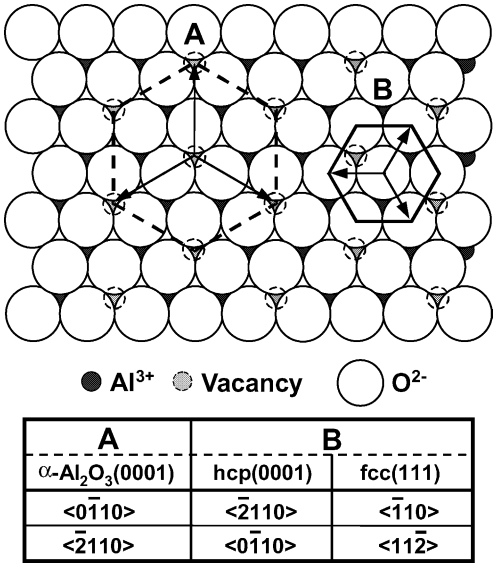

Fig. 6. Schematic diagram and orientation of a reconstructed oxygen-terminated α-Al_2O_3(0001) surface: the bulk unit cell (A; dotted line) and surface unit cell (B; solid line), are identical with fcc(111) and hcp(0001) planes.

Fig. 7 shows schematically the configuration of Cr and oxygen atoms—adjacent to the interface—for NW(OR-I) and KS(OR-II) ORs, which are identical to OR-IT and OR-IIT, respectively. In the case of the NW

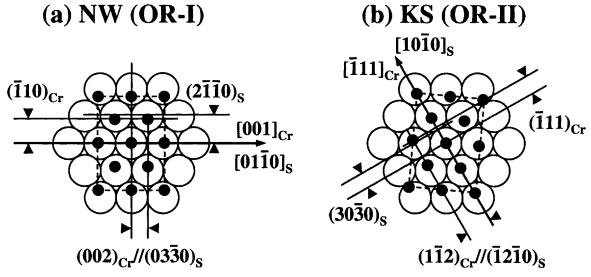

Fig. 7. Configuration of Cr atoms on the dense-packed oxygen surface: (a) OR-I (NW) with low lattice mismatch between $(002)_{Cr}$ and $(03\text{-}30)_S$, and (b) OR-II (KS) with low mismatch between $(1\text{–}12)_{Cr}$ and $(-12\text{–}10)_S$.

orientation, $[001]_{Cr}//[01\text{–}10]_S$ [Fig. 7(a)] and in the case of the KS orientation, $[\bar{1}11]_{Cr}//[10\text{–}10]_S$ [Fig. 7(b)].

Different geometrical approaches can be used to predict the formation of epitaxial orientation relationships between films and substrates: (i) the lattice mismatches between different in-plane directions between film and substrate, (ii) a rigid lattice approximation on the basis of atomic radii of the atoms of film and substrate[34,35] and (iii) two dimensional near coincidence site lattices (NCSL[40–43]). In the following, we will discuss the approaches (i) and (ii). A description of the orientation relationships in terms of NCSL[40–43] will follow in a separate paper which will include a comparison of different metal/sapphire systems.

(i) For the above given KS and NW orientation, we calculated the lattice mismatches $f(\%)$ between the corresponding planes of sapphire and a variety of bcc metals, including Cr (Table 1). In the case of Cr/α-Al_2O_3(0001), the NW and KS orientations exhibit a pair of lattice planes with a fairly low lattice mismatch, i.e. $f=-4.8\%$ between $(001)_{Cr}$ and $(03\text{–}30)_S$ planes (NW) and $f=1\%$ between $(1\text{–}12)_{Cr}$ and $(-12\text{–}10)_S$ planes (KS). It is believed that both orientations are stabilized by these low interfacial lattice mismatches. In the case of Nb/α-Al_2O_3(0001), OR-I (NW) was observed experimentally under some special growth conditions. The occurrence of this orientation relationship is also favored by a low lattice mismatch (Table 1). However, due to high lattice mismatches, OR-II (KW) is not feasible in the Nb/α-Al_2O_3(0001) system. From the present results it can be concluded that lattice mismatches below 10% will favor the NW orientation. Except for Nb, for all metals displayed in Table 1, small mismatch directions can be found which will favor the KS orientation. Furthermore, the mismatches of the different metals have negative or positive sign, indicating that small coherent or partially coherent clusters will be under compression or tension. Presently, the influence of the sign of the stress on the development of special orientation relationship is unclear.

(ii) The formation of NW and KS orientations can also be predicted by a geometrical model on the basis of a rigid lattice approximation, by calculating the following ratio,

$$r = d_{bcc}/d_{fcc}$$

where d_{bcc} and d_{fcc} represent the atomic radii of the bcc and fcc metals, respectively.[34,35] For the NW configuration, $0.82<r<0.87$ (NW-1) and $1.03<r<1.15$ (NW-2) are expected, whereas $0.89<r<1.01$ will favor the KS configuration.[34] Table 2 shows the values of lattice constants and atomic radii d_{bcc} (one half of the interatomic distance) for bcc metals,[44] and the ratio $r=d_{bcc}/d_O$, where d_O is the oxygen ion radius (1.38 Å).[45] Nb[4,9,10] and Mo[14] exhibited the NW orientation, while Fe [46] grew with the KS orientation. The value of r ranged from 0.90 for Fe, with the smallest atomic radius (1.24 Å) to 1.04 for Nb with the largest radius (1.43 Å). For Cr, $r=0.91$. This value falls within the range where one would expect the formation of the KS orientation. Both relationships, NW and KS, however, were observed in the present study. For the Cr(110)/Pd(111) system, Hellwing et al. [47] calculated $r=0.91$. These authors also observed the formation of NW and KS orientations at low growth temperatures. Most likely, these orientations are formed during relaxation of clusters which are coherently strained in the very initial growth stage.

Table 2
Experimentally determined orientation relationships between bcc metals (110) and α-Al_2O_3(0001), and geometrical parameters of bcc metals (lattice constants, atomic radii d_{bcc}, and the ratio r of d_{bcc} to oxygen ionic distance $d_O=1.38$ Å)

Metal (bcc)	Nb	Mo	V	Cr	Fe
Lattice constant (Å)	3.31	3.15	3.03	2.88	2.87
Atomic radius d_{bcc} (Å)	1.43	1.36	1.31	1.25	1.24
Radius ratio r (d_{bcc}/d_O)	1.04	0.99	0.95	0.91	0.90
Experimental OR [reference]	NW [4,7,9–12]	NW [14]	–	NW + KS [this study]	KS [46][a]

[a] Orientation relationship of Fe precipitates in α-Al_2O_3.

5. Conclusions

The present results suggest that the coexistence of the NW and KS orientations is favored by relatively low lattice mismatches along individual in-plane directions (Table 1) between the Cr film and the α-Al_2O_3 substrate. Presently, no detailed information is available about the nucleation of Cr on the α-Al_2O_3 (0001) surface. However, the formation of different, well-defined orientations indicates that Cr grows in the form of three-dimensional islands, i.e. isolated nuclei are formed in the very initial growth stage. Provided that the α-Al_2O_3 (0001) surface is oxygen-terminated, the Cr atoms may preferably adsorb on top of oxygen atoms. This behavior is also found for other metal/oxide systems (e.g. [48]). We think that in the individual growth stage, Cr clusters grow full coherent with the substrate. With increasing cluster size, relaxations are taking place along directions with high lattice mismatches. The formation of KS and NW orientations is therefore based on low lattice mismatches between $(1\text{–}12)_{Cr}$ and $(-12\text{–}10)_S$ and $(002)_{Cr}$ and $(03\text{–}30)_S$, respectively. For the system it seems to be energetically favorable to keep the corresponding in-plane directions between Cr and α-Al_2O_3 parallel. A further thickening of islands will finally result in the relaxation along these low mismatch directions and in the occurence of the KS and NW ORs.

References

1. Wagner, T., Marien, M. and Duscher, G., *Thin Solid Films*, 2001, **398/399**, 419.
2. Wagner, T., Richter, G. and Rühle, M., *J. Appl. Phys*., 2001, **89**, 2606.
3. Bernath, S., Wagner, T., Hofmann, S. and Rühle, M., *Surface Science*, 1998, **400**, 869.
4. Cuomo, J. J. and Angilello, J., *J. Electrochem. Soc*., 1973, **120**, 125.
5. Durbin, S. M., Cunningham, J. E., Mochel, M. E. and Flynn, C. P., *J. Phys*., 1981, **F11**, L223.
6. Durbin, S. M., Cunningham, J. E. and Flynn, C. P., *J. Phys*., 1982, **F12**, L75.
7. Claassen, J. H., Wolf, S. A., Qadri, S. B. and Jones, L. D., *J. Cryst. Growth*, 1987, **81**, 557.
8. Mayer, J., Finnis, C. P. and Rühle, M., *Ultramicroscopy*, 1990, **33**, 51.
9. Wagner, T., Lorenz, M. and Rühle, M., *J. Mater. Res*., 1996, **11**, 1255.
10. Wagner, T., *J. Mater. Res*., 1998, **13**, 693.
11. Wildes, A. R., Mayer, J. and Theis-Bröhl, K., *Thin Solid Films*, 2001, **401**, 7.
12. Masek, K. and Matolín, V., *Thin Solid Films*, 1998, **317**, 183.
13. Knowles, K. M., Alexander, K. B., Somekh, R. E. and Stobbs, W. M., *(EMAG 87) Inst. Phys. Conf. Series*, 1987, **90**, 245.
14. Igarashi, O., *Jpn. J. Appl. Phys*., 1995, **34**, L563.
15. Ikuhara, Y. and Pirouz, P., *Ultramicroscopy*, 1993, **52**, 421.
16. Biener, J., Bäumer, M., Madix, R. J., Liu, P., Nelson, E., Kendelewisz, T. and Brown Jr., G., *Surf. Sci*., 2000, **449**, 50.
17. Mckenzi, D. R., *Appl. Phys. Lett*., 1979, **34**, 25.
18. Schröder, K. and Hejase, H., *Phys. Stat. Sol. (b)*, 1988, **149**, 685.
19. Moore, J. P., Williams, R. K. and Graves, R. S., *J. Appl. Phys*., 1977, **48**, 610.
20. Bretzger, B. *et al*., *J. Vac. Sci. Technol. B*, 1997, **15**, 7080.
21. Ekardt, Walter., ed., *Metal Clusters*. Wiley Series in Theoretical Chemistry, Wiley, Weinheim, 1999.
22. Romanov, A. E. and Wagner, T., *Scripta Mat*., 2001, **45**, 325.
23. Strecker, A., Salzberger, U. and Mayer, J., *Prakt. Metallogr*., 1993, **30**, 481.
24. Pashley, D. W., Materials Science and Technology. In *Processing of Metals and Alloys*, ed. R. W. Cahn, P. Haasen and E. J. Kramer. VCH, Weinheim, 1991, pp. 289.
25. Venables, J. A., *Introduction to Surface and Thin Film Processes*. Cambridge University Press, Cambridge, 2000.
26. Haas, G., Menck, A., Brune, H., Barth, J. V., Venables, J. A. and Kern, K., *Phys. Rev. B*, 2000, **61**, 11105.
27. Reed, T. B., *Free Energy Formation of Binary Compounds: An Atlas of Charts for High-Temperature Chemical Calculations*. MIT Press, 1971.
28. Gautier, M., Renaud, G., Pham Van, L., Villette, B., Pollak, M., Thromat, N., Jollet, F. and Duraud, J. P., *J. Am. Ceram. Soc*., 1994, **77**, 323.
29. Ohuchi, F. S. and Kohyama, M., *J. Am. Ceram. Soc*., 1991, **74**, 1163 (and references therein).
30. Tasker, P. W., *Adv. Ceram*., 1984, **10**, 176.
31. French, T. M. and Somorjai, G. A., *J. Phys. Chem*., 1970, **74**, 2489.
32. Kruse, C., Finnis, M. W., Milman, V. Y., Payne, M. C., Vita, A. D. and Gillan, M. J., *J. Am. Ceram. Soc*., 1994, **77**, 431.
33. Scheu, C., Dehm, G. and Rühle, M., *Phil. Mag. A*, 1998, **78**, 439.
34. Bruce, L. A. and Jaeger, H., *Phil. Mag. A*, 1978, **38**, 223.
35. Bauer, E. and Van der Merwe, J., *Phys. Rev. B*, 1986, **33**, 3657.
36. Wassermann, G., *Arch. Einsenhüttenwesen*, 1933, **126**, 647.
37. Nishiyama, Z., *Sci. Rep., Tohoku Univ*., 1934, **23**, 638.
38. Kurdjumov, G. and Sachs, G., *Z. Phys*., 1930, **64**, 325.
39. Grigorov, I. L., Fitzsimmons, M. R., Siu, I.-L. and Walker, J. C., *Phys. Rev. Lett*., 1999, **82**, 5309.
40. Balluffi, R. W., Brokman, A. and King, A. H., *Acta Metall*, 1982, **30**, 1453.
41. Hwang et al, D. M., *Appl. Phys. Lett*., 1990, **57**, 1690.
42. Dickey, E. C., Ma, Y., Bagiyono, G., Lian, D., Sinnott, S. B. and Wagner, T., *Thin Solid Films*, 2000, **372**, 37.
43. Gao, Y., Shewmon, P. and Dregia, S. A., *Scripta Metall*., 1988, **22**, 1521.
44. Pearson, W. B., ed., *A Handbook of Lattice Spacings and Structures of Metals and Alloys*. Pergamon Press, 1967.
45. Chiang, Y. M., Birnie, D., Kingery, W. D., ed., *Physical Ceramics: Principle for Ceramic Science and Engneering*. John Wiley & Sons, 1997.
46. Moon, A. R. and Phillips, M. R., *J. Am. Ceram. Soc*., 1991, **74**, 865.
47. Hellwig, O., Bröhl, K. T., Wilhelmi, G., Zabel, H. and Stierle, A., *Thin Solid Film*, 1998, **318**, 201.
48. Ochs, T., Köstlmeier, S. and Elsässer, C., *Integrated Ferroelectrics*, 2001, **32**, 267; Ochs, T. and Elsässer, C., *Z. Metallkunde*, 2002, **93**, 406.